Synthesis, structural, and optical characterizations of zinc oxide: silver oxide nanoparticles conjunction with polymer polyvinylpyrrolidone

S. S. Hamood[a,*], M. S. Khalaf[b], F. S. Mohammed[a]
[a]*Physics department, college of science, Mustansiriyah University, Baghdad-Iraq*
[b]*Ministry of Science and Technology, Directorate of treatment of Military, Biological, and Chemical, Disposal, Baghdad-Iraq*

Pulsed laser ablation (PLA) technology has been utilized for creating nano-sized particles from silver oxide, zinc oxide, and mixed oxide (Ag_2O, ZnO, ZnO: Ag_2O) combined with polyvinylpyrrolidone (PVP) for environmental applications, especially the filtration regarding oil-polluted water in rivers. A range of analytical methods have been employed to describe the prepared as well as polymer-supported nanomaterials' characteristics. Energy-dispersive X-ray spectroscopy, scanning \ transmission electron microscopy (SEM \ TEM) analysis, X-ray diffraction \ fluorescence (XRD \ XRF), Fourier-transform infrared spectroscopy, and photoluminescence measurements (PL) were among them. The nanocomposite ZnO: Ag_2O showed numerous nanostructures with diverse orientations, according to XRD analysis. SEM imaging of the Ag_2O nanoparticles indicated polydispersed spherical particles with widespread aggregation. Furthermore, the study incorporated the use of polymer-supported nanomaterials, with PVP selected for its excellent chemical and thermal resistance. Various membrane structures with differing porosities were prepared and effectively employed for the filtration of oil-polluted water, as validated through TEM, XRF, and other measurements. In this context, the polymer functioned akin to a sponge for water pollution remediation.

(Received June 23, 2024; Accepted September 9, 2024)

Keywords: Zinc oxide nanoparticles, Silver nanoparticles, Pulsed laser ablation, Antibacterial

1. Introduction

In a wide range of domains, nanotechnology has made significant scientific advancements [1] [2]. Significant novel products have been introduced in pharmaceuticals as a result of nanotechnological advancements [3-5]. In its nanostructured form, ZnO, an inorganic compound insoluble in water, demonstrates strong antimicrobial capabilities [7]. From baby powder to skin ointments, anti-dandruff shampoos, sunscreen, and oil, it is utilized in a broad range of healthcare and medical applications [8–11]. ZnO ointment is useful for treating a variety of skin diseases that are prone to infection, including burns, insect bites, eczema, and diaper rash in infants [12–16]. Comparably, Ag_2O, an additional powerful antimicrobial compound [17, 19], has extensive applications in medicine. Decreasing the size of Ag_2O particles, on the other hand, may cause them to aggregate, which would greatly affect their antibacterial and chemical activity [20]. It is hypothesized that ZnO and Ag_2O could work in concert to create nanocomposites with enhanced anticancer and antibacterial properties. It was demonstrated that adding metals or metal oxides lowers band gaps, enhancing antibacterial activity [21]. When ZnO is doped with silver, the inhibitory action of pure ZnONPs is significantly increased. Composite nanomaterials might inherit characteristics from the elements that make them up, which could lead to synergistic effects [22]. According to reports, Ag_2O's shape could alter its catalytic properties and the antibacterial effects that follow [23][24]. PVP is unique in that it is a temperature-resistant, pH-stable, nontoxic, non-ionic, and inert polymer with affinities for both hydrophobic and hydrophilic medications. Originally utilized as a plasma volume expander during the 1940s, PVP has discovered numerous uses in the food sector, cosmetics, biomedicine, and pharmaceuticals [25].

* Corresponding author: sarasameer@uomustansiriyah.edu.iq
https://doi.org/10.15251/DJNB.2024.193.1291

Accidental oil spills in water bodies are frequent incidents resulting from the transportation and extraction of oil through wells, drilling platforms, rigs, pipelines, and tanks. These incidents pose significant environmental risks, necessitating immediate and efficient decontamination measures to safeguard the environment and aquatic ecosystems. Conventional oil spill cleanup methods struggle to fully separate oil and water. Nanotechnology, including sol-gel, hydrothermal, and pulsed laser ablation (PLA) techniques, is showing promise for more effective oil spill remediation [26–29]. PLA offers notable advantages, including the production of well-crystallized NPs devoid of by-products, cost-effective ablation control, and adjustable material size through parameter manipulation [31].

This work examines the anticancer and antibacterial characteristics of undoped zinc oxide as well as ZnO: Ag_2O nanocomposite that was produced using PLA. Comprehensive research has been done on the physicochemical properties of the produced NPs, including their solid phase, morphology, and dynamic particle sizes [32][33].

2. Materials and methods

With the use of a pulsed Nd: YAG laser (HUAFEI) with a wavelength of 1064nm, Ag_2O, ZnO, and ZnO: Ag_2O NPs have been produced. Through irradiating a ZnO pellet that was positioned at the bottom of a quartz vessel that held 1.5 ml of solution above the target, colloidal solutions were prepared. A 10Hz repetition rate, fixed laser energy of 200mJ/pulse, and a pulse width of ns were the laser parameters. A Joule meter has been utilized for measuring the amount of laser energy that reached the surface throughout the six-minute ablation process. The laser beam was concentrated at a spot size of 2.3 mm with the use of a converging lens with a 10cm focal length. Fig.1 displays a diagram of the laser ablation apparatus used in this investigation. The same laser parameters were then used for ablating an Ag plate of the same size in order to produce Ag_2O colloids for 600 pulses. Polyvinylpyrrolidone (PVP) was employed in the synthesis of Ag_2O, ZnO, and ZnO: Ag_2O NPs for comparing the processes. PVP weighing 0.5 g was dissolved in each material. Then, 1.5 ml of deionized water containing 5 g of polymer was mixed with each of the nanomaterials, whether they had been prepared without or with PVP. Polymer films were formed when the mixture was allowed to dry [34].

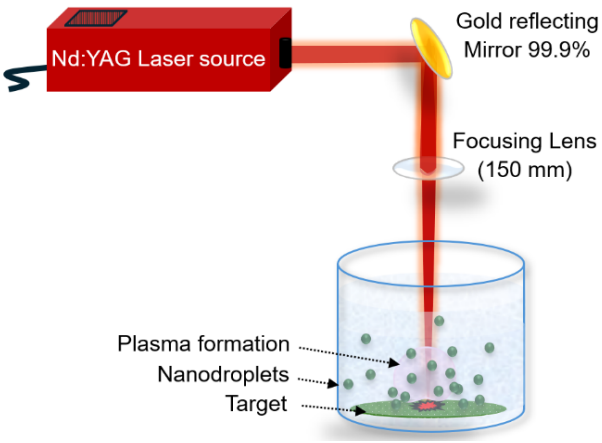

Fig. 1. PLAL setup and Synthesis process of ZnO: Ag_2O nanostructures.

3. Results and discussion

3.1. X-ray diffraction spectroscopy

Figure 2 shows the ZnO NPs that were produced and their XRD patterns. The XRD patterns regarding ablated Ag_2O show peaks at 2θ = 38.24°, 44.28°, 64.54°, 77.46°, and 81.48°, which match the information found on card 04-0783 in the JCPDS file for face-centered cubic Ag_2O NPs [35]. Additionally, six peaks can be seen in XRD patterns displayed in Fig. 4-1, which are situated at 31.86°, 34.52°, 36.35°, 47.66°, and 56.71°. The hexagonal wurtzite structure of ZnO (JCPDS card no. 36-1451) is responsible for all of the XRD peaks of ZnO NPs, demonstrating an extraordinary degree of crystal quality. Furthermore, two sets of diffraction peaks are clearly visible in Fig. 4-1's XRD pattern of Ag_2O: ZnO nanostructure. These sets include XRD peaks of ZnO as well as Ag_2O, which unmistakably correspond to face-centered structure regarding Ag_2O (JCPDS card no. 04-0783) as well as hexagonal wurtzite structure of ZnO (JCPDS card no. 36-1451). Diffraction peaks of Ag_2O as well as ZnO in Ag_2O: ZnO NPs notably do not move, conclusively indicating the lack of diffraction from other impurities.

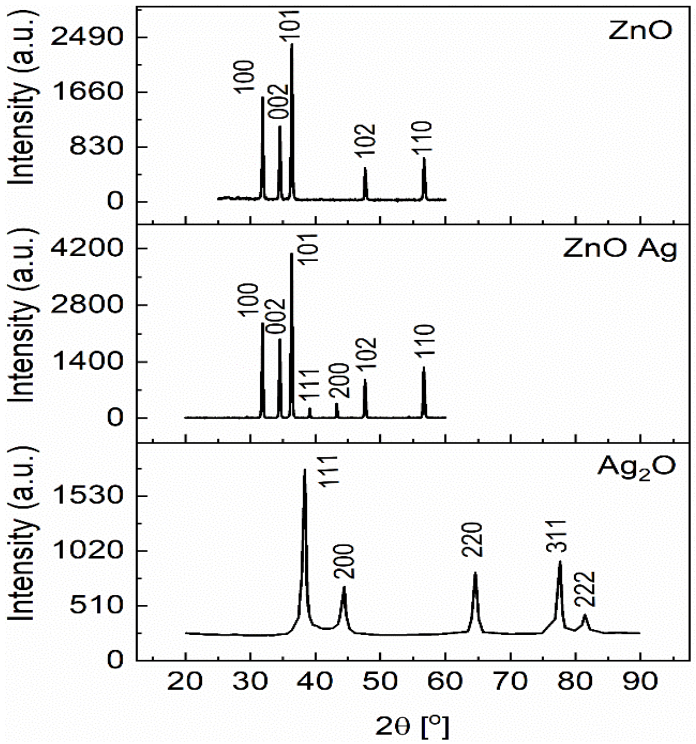

Fig. 2. XRD Patterns of zinc oxide, silver and mix zinc oxide: sliver nanoparticles.

3.2. Fourier-transform infrared spectroscopy

The identification of functional groups is greatly aided by FTIR spectroscopy. ZnO absorption band is depicted in Fig. 3, where peaks are found at 1644.30, 2954.43, 2895.97, and 3392.86 cm^{-1}, which represent the C=O, CH, and NH groups, respectively. Ag_2O NPs' FTIR absorption spectra show large NH absorption-related absorption peaks at 3391.48 and 3307.46 cm^{-1}. The extended vibrations at 3273.30 cm^{-1} correspond to amine (OH) groups, while the band at 1644.71 cm^{-1} relates to C=O stretching modes. The spectra also show C–H stretching (alkanes) and O–H stretching (alcohols) at 2965.42 and 2920.27 cm^{-1}. Comparably, ZnO: Ag_2O NPs' FTIR absorption spectra reveal that NH stretching (amines) occurs at around 3393.38cm^{-1}, whereas C–H stretching (alkanes) is found at 2964.44cm^{-1}. Regarding Ag_2O: ZnO, a strong band at 493 and 428

cm^{-1} is ascribed to vibratory ZnO elongation and deformation, respectively, whereas an absorption band at 1644.13 cm^{-1} suggests C=O stretching. PVP's absorption band also shows peaks at 1644.19, 2953.32, 2895.34, 2928.71, and 3392.71cm^{-1}, which represent the C=O, CH, and NH groups, respectively. The C=O, CH, and NH groups are responsible for the peaks in the ZnO: PVP absorption band, which are located at 1644.38, 2895.70, 2954.19, 3294.53, and 3392.03 cm^{-1}. Lastly, large absorption peaks at 3393.80, 3273.56, 2953.20, 2927.85, and 2348.17 cm^{-1} are visible in the FTIR absorption spectrum of Ag_2O: PVP NPs, corresponding to the C=C, OH, CH, and NH groups. Comparably broad absorption peaks are seen in the FTIR absorption spectrum of ZnO: Ag_2O: PVP NPs at 3392.32, 2954.40, 2895.82, and 1644.18 cm−1, which correspond to the C=O, OH, CH, and NH groups, respectively.

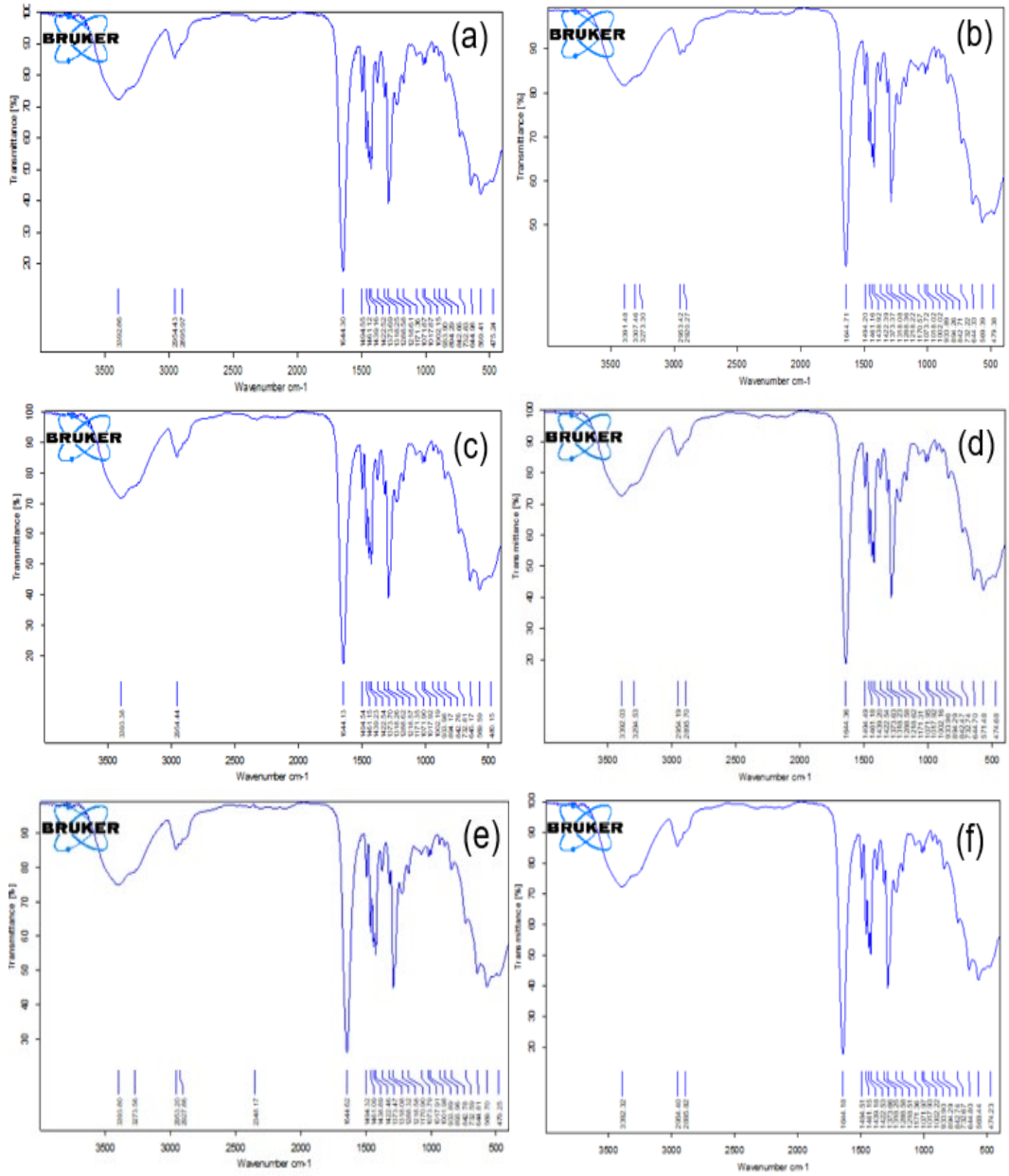

Fig. 3. FTIR of (a) ZnO, (b) Ag_2O and (c) ZnO: Ag_2O Nps, (d) ZnO:PVP, (e) Ag_2O:PVP and (f) ZnO:Ag_2O:PVP NPs.

3.3. Photoluminescence spectroscopy

Fig. 4-4 presents photoluminescence measurements as a function of wavelength for ZnO, Ag_2O, and ZnO: Ag_2O NPs synthesized via laser ablation in water at room temperature. The emission wavelengths observed in Fig. 4-4 are 430 nm for ZnO, 485 nm for Ag_2O, and 440 nm for ZnO: Ag_2O. These wavelengths signify the recombination processes between electrons and the holes generated by photon emission. The doping of silver in various configurations and the appearance of crystal defects brought on by oxidation processes during the laser ablation deposition process in water are the reasons for this increase in electron concentration.

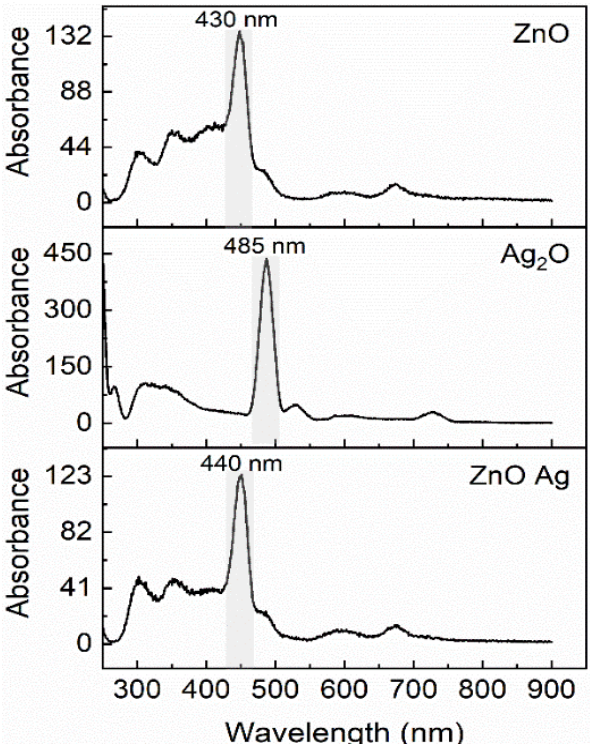

Fig. 4. PL images of (ZnO NPs), (Ag_2O NPs) and (ZnO: Ag_2O NPs).

3.4. Scanning electron microscopy

In Fig. 4-5, SEM images of the ZnO, ZnO: Ag_2O, and Ag_2O NP films are presented, showcasing a smooth and homogeneously distributed surface with very fine crystallites. When Ag_2O NPs are added to the primarily ZnO NP surface, it has been observed that the particle size rises. The resulting coating was homogenous and conformal, covering the whole surface of the samples under investigation, according to SEM examination. The ZnO layers showed a smooth morphology without any breaks, cracks, gaps, or imperfections. Additionally, the synthesized nanoparticles formed spherical shapes of different sizes due to stable mass distribution and colloid formation. Based on SEM images, the particle sizes ranged from 10 to 50 nm.

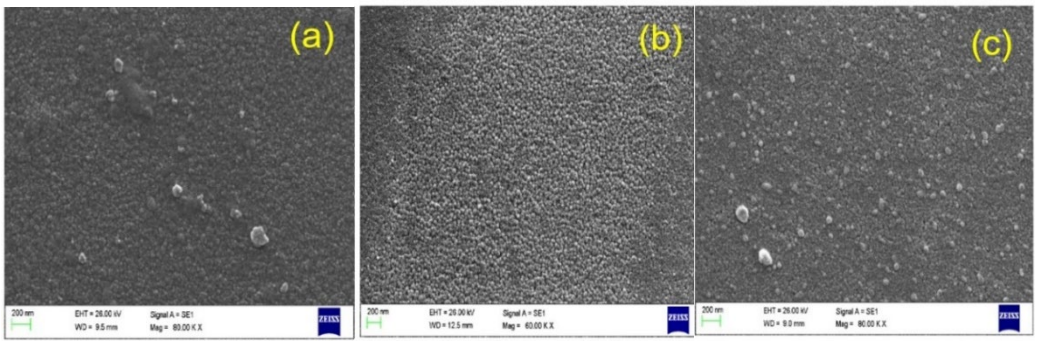

Fig. 5. Scanning Electron Microscope (SEM) images for ZnO NPs, Ag_2ONPS, and ZNO: Ag_2ONPs.

3.5. Transmission electron microscopy

The Ag_2O, ZnO, and ZnO: Ag_2O NPs TEM images of nanocrystal formation are shown, together with PVP, ZnO: Ag_2O: PVP, ZnO: PVP, and Ag_2O: PVP filters. The nanomaterials are less than 50 nm on average. Fig. 4-6 shows a TEM micrograph that reveals spherical forms and a limited particle size distribution. Following the creation of the nanomaterial with PVP, the surface porosity of the samples was evaluated again, and this time it was higher due to the addition of polymer throughout the laser ablation procedure. As a result, the samples' surface area increased.

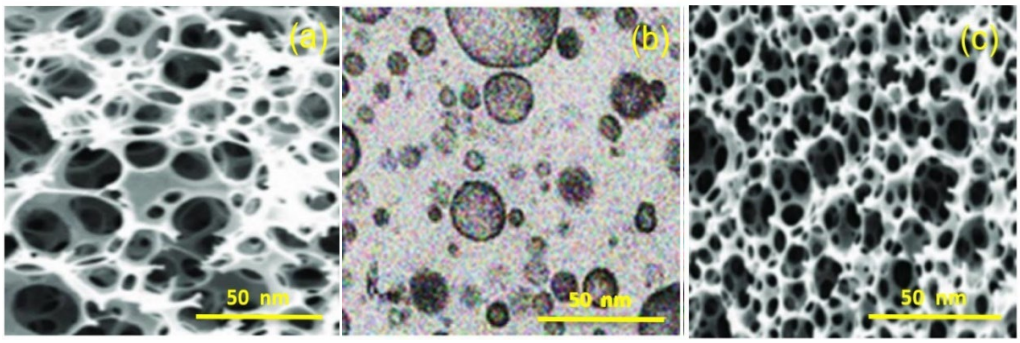

Fig. 6. TEM images of nanocrystal formation of ZnO: Ag_2O NPS, (a) ZnO:PVP, (b) Ag_2O:PVP. (c) ZnO:Ag_2O:PVP,

3.6. X-ray energy-dispersive

The elemental compositions of ZnO, Ag_2O, and ZnO: Ag_2O nanostructures, EDX analysis was carried out as can be seen in Figs 4-8 (A) and (B). The EDX analysis of the NPs provided the atomic percentage (%) of elements such as Zn, O, and Ag, which are apparent in the images, reflecting the composition of the samples containing mainly Zn and oxygen. Similar results were obtained for the mixture sample, showing that no other elements were present.

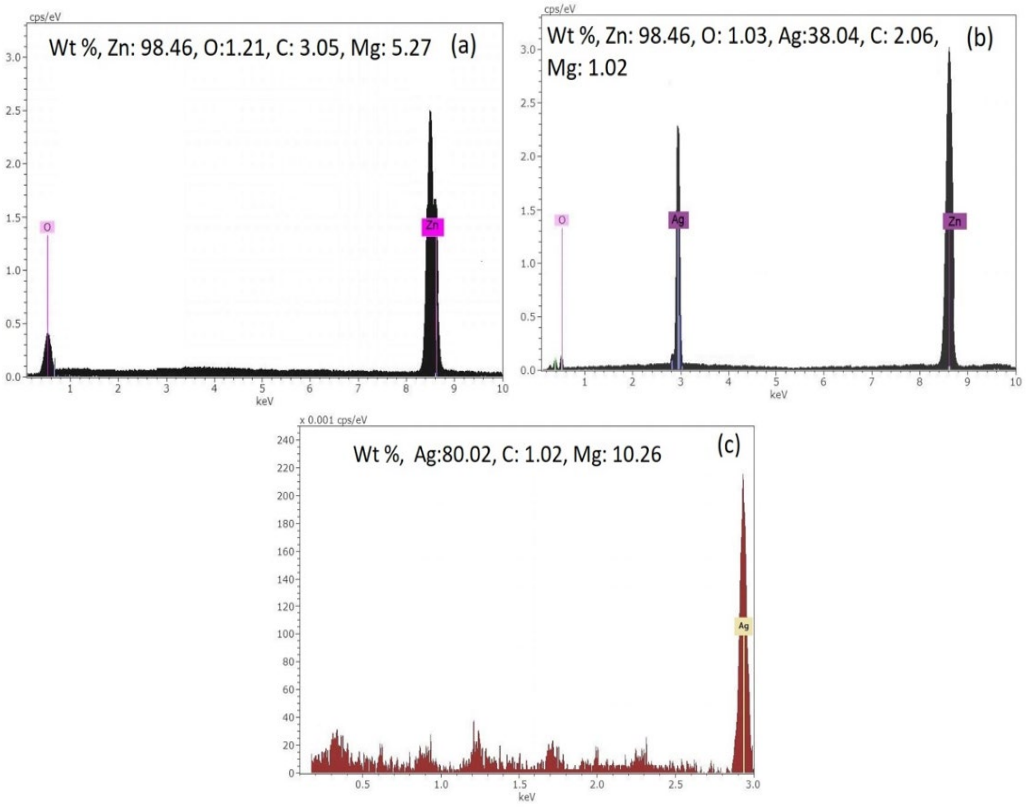

Fig. 7. EDX Spectrum of (A) ZnO,(B): Ag_2O NPs and (C): ZnO: Ag_2O NPs.

3.7. X-ray fluorescence spectroscopy

The proportions of elements in water contaminated with oil and other substances were measured after performing the filtration process. Table 4-5 shows the X-ray fluorescence (XRF) results for water contaminated with oil. It can be seen from the table that the oil-contaminated water contains many elements, including carbon, phosphorous, phosphate, silver, potassium, iron, sodium, and magnesium. The highest percentage was obtained for carbon. The other table shows the elements after the filtering process. The formula of the oil is

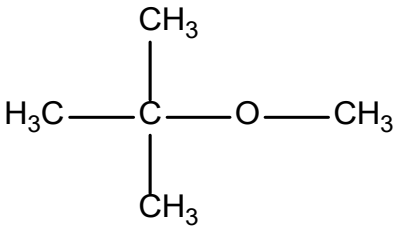

Table 1. The XRF for polluted.

Elements	Wt. (%)			
	Mineral Oil and after filtration	**Mineral Oil after ZnO/Flitter**	**Mineral Oil after Ag_2O/Flitter**	**Mineral Oil after ZnO:Ag_2O/Flitter**
C	12	10	9	3
O	5	3	9	10
B	8	3	2	-
Fe	70	40	20	36
P	0.4	0.1	-	-
Ca	0.5	0.4	0.3	-
Cr	-	0.3	0.1	-
Zn	-	1.0	1.2	1.1
Ce	-	-	-	0.1

4. Conclusion

ZnO, Ag_2O, and ZnO: Ag_2O NPs were successfully synthesized, with and without PVP, using the laser ablation method. These NPs were explored for their potential applications in environmental purification. Analysis via XRD patterns revealed sharp peaks, indicating the absence of impurities in the prepared samples. SEM images depicted uniformly shaped particles for Ag_2O, ZnO, and ZnO: Ag_2O NPs. TEM electron microscopy further confirmed the favourable shape and structure of the resulting nanomaterials. Measurements conducted before and after using the nanomaterials yielded promising results, highlighting the efficacy of PVP as it functioned akin to a sponge for pollutants present in water.

This study underscores the significance of PVP, a widely used material in synthesizing microfiltration and ultrafiltration membranes. PVP boasts excellent chemical and thermal resistance across a wide pH range. By varying polymer properties and the additive-to-polymer ratio, membranes with diverse morphologies (pore structures) and hydrophilic properties can be finely tuned, influencing performance factors such as permeability, rejection rates, and resistance to fouling.

Acknowledgments

The Dept. of Physics staff at the Laboratory of Advanced Materials, College of Science, Mustansiriyah Univ., is acknowledged and thanked by the authors for taking the necessary measurements.

References

[1] A. Rahdar, S. Rahdar, G. Labuto, Environ. Sci. Pollut. Res., 27(9), 9181-9191(2020); https://doi.org/10.1007/s11356-019-07491-y
[2] M.E.T. Yazdi, J. Khara, M.R. Housaindokht, H.R. Sadeghnia, S.E. Bahabadi, M.S. Amiri, H. Mosawee, D. Taherzadeh, M. Darroudi, IET nanobiotechnology, 13(2), 189 (2019); https://doi.org/10.1049/iet-nbt.2018.5215
[3] O.M. Abdulmunem, E.S. Hassan, J. Opt., (2024); https://doi.org/10.1007/s12596-024-01943-6
[4] Hussein, G.A.A., Mohammed, F.S.December. AIP Conference Proceedings, 2290 (1), (2020); https://doi.org/10.1063/5.0028990
[5] H. Sharifan, J. Moore, X. Ma, Ecotoxicol. Environ. Saf., 191, 110177(2020); https://doi.org/10.1016/j.ecoenv.2020.110177

[6] P. Sivakumar, M. Lee, Y.S. Kim, M.S. Shim, J. Mater. Chem. B., 6(30), 4852-4871(2018); https://doi.org/10.1039/C8TB00948A
[7] T. Holland, A.M. Abdul-Munaim, D.G. Watson, D.G., P. Sivakumar, Lubricants, 7(1), 4 (2019); https://doi.org/10.3390/lubricants7010004
[8] N. Geetha, S. Sivaranjani, A. Ayeshamariam, J. Suthan Kissinger, M. Valan Arasu, M. Jayachandran, Fluid Mech. Open Acc, 3, 141(2016); https://doi.org/10.4172/2476-2296.1000141
[9] K. Ravichandrika, P. Kiranmayi, R. Ravikumar, Int J App Pharm, 10(6), 224-8(2018); https://doi.org/10.22159/ijap.2018v10i6.29376
[10] G.J. Nohynek, E.K. Dufour, Arch. Toxicol., 86, 7 (2012); https://doi.org/10.1007/s00204-012-0831-5
[11] X. Ma, H. Sharifan, F. Dou, W. Sun, Chem. Eng. J., 384, 123802 (2020). https://doi.org/10.1016/j.cej.2019.123802
[12] B. Birkenstock, Brauwelt International, 28, (6/10), 351-352(2010)
[13] L. H. Amundson, M. C. Richard, Family medicine: principles and practice, New York, NY: Springer New York, 1074-1144 (1983); https://doi.org/10.1007/978-1-4757-4002-8_73
[14] Z. Saremi, R. Yari, I. Khodadadi, S.M. Tabatabaei, J. Skin Stem Cell, 3, 4 (2016); https://doi.org/10.5812/jssc.66329
[15] P. Uikey, K. Vishwakarma, Int. J. Emerg. Technol Comput. Sci Electron, 21(2), 239-42(2016)
[16] A.K. Barui, R. Kotcherlakota, C.R. Patra, Inorganic Frameworks as Smart Nanomedicines Elsevier, Amsterdam, 239 (2018)
[17] P. Pardeshi, A. Nawale, V. Mathe, Y. Lahir, P. Dongre, Bio Nano Front, 2, 176-180 (2014)
[18] Z. Hu, W.L. Chan, Y.S. Szeto, J. Appl. Polym. Sci., 108(1), 52-56 (2008); https://doi.org/10.1002/app.26822
[19] Tripathi, Shipra, G. K. Mehrotra, P. K. Dutta, Bulletin of Materials Science, 34, 29-35 (2011); https://doi.org/10.1007/s12034-011-0032-5
[20] R.S. Sabry, A.M. Abbas, F.S. Mohammed, W.J. Aziz, Journal of Materials Science: Materials in Electronics, 27(4), 3170-3174 (2016); https://doi.org/10.1007/s10854-015-4141-6
[21] G.Y. Nigussie, G.M.Tesfamariam, B.M.Tegegne, Y.A. Weldemichel, T.W. Gebreab, D.G. Gebrehiwot, G.E. Gebremichel, Int. J. Photoenergy, 2018, (2018); https://doi.org/10.1155/2018/5927485
[22] B.B. Fonseca, P.L.A.P.A. Silva, A.C.A. Silva, N.O. Dantas, A.T. Paula, O.C.L. Olivieri, M.E. Beletti, D.A. Rossi, L.R. Goulart, Front. Microb, Front. Microb., 10, 217 (2019); https://doi.org/10.3389/fmicb.2019.00217
[23] X. Wang, H.F. Wu, Q. Kuang, R.B. Huang, Z.X. Xie, L.S. Zheng, Langmuir, Mater. Lett. 26(4), 2774-2778 (2010); https://doi.org/10.1021/la9028172
[24] L. A.-H. Said, Al-Mustansiriyah Journal of Science, 31(3), 1–5 (2020); https://doi.org/10.23851/mjs.v31i3.361
[25] K. M. Koczkur, S. Mourdikoudis, L. Polavarapu, S. E. Skrabalak, Dalton transactions, 44(41), 17883-17905 (2015); https://doi.org/10.1039/C5DT02964C
[26] P. Mahajan, S. Dhoke, A. Khanna, Journal of Nanotechnology, 2011, (2011); https://doi.org/10.1155/2011/696535
[27] Jubear, S. K., Abdulmunem, O. M., Hassan, E. S. Digest Journal of Nanomaterials & Biostructures (DJNB), 19(1), (2024); https://doi.org/10.15251/DJNB.2024.191.97
[28] F. Razi, S. Zinatloo-Ajabshir, M. Salavati-Niasari, Journal of J. Mol. Liq. 225, 645-651(2017); https://doi.org/10.1016/j.molliq.2016.11.028
[29] S. A.H.Abbas, E. S. Hassan, O.M. Abdulmunem, Baghdad Sci. J., (2023); https://doi.org/10.21123/bsj.2023.8336
[30] H.S. Al-Salman, M.J. Abdullah, Measurement, 59, 248-257(2015); https://doi.org/10.1016/j.measurement.2014.08.011
[31] O. Abdulmunem, K. Hassoon, M. Gaafar, A. Rahimi-Iman, A., J.C Balzer, Millimeter and Terahertz Waves, 38, 1206-1214 (2017); https://doi.org/10.1007/s10762-017-0412-z
[32] E. S. Hassan, O. M. Abdulmunem, Brazilian Journal of Physics, 52(5), 160 (2022); https://doi.org/10.1007/s13538-022-01158-9

[33] A. M. Rasheed, H. H. Al-Shammary, Al-Mustansiriyah Journal of Science, 31(3), 21–27 (2020); https://doi.org/10.23851/mjs.v31i3.732
[34] Zhang, Shuai et al., Applied Physics B, 126(8), 1-9, (2020); https://doi.org/10.1007/s00340-020-07490-9
[35] G. Nagaraju, S. Prashanth, M. Shastri, K. Yathish, C. Anupama, D. Rangappa, Materials Research Bulletin, 94, 54-63 (2017); https://doi.org/10.1016/j.materresbull.2017.05.043